ESI for

Phosphorescence Doping in a Flexible Ultramicroporous Framework for High and Tunable Oxygen Sensing Efficiency

Xiao-Lin Qi,[a] Si-Yang Liu,[a] Rui-Biao Lin,[a] Pei-Qin Liao,[a] Jia-Wen Ye,[a] Zhihui Lai,[b] Yanyan Guan,[b] Xiao-Ning Cheng,[b] Jie-Peng Zhang*[a] and Xiao-Ming Chen[a]

[a] MOE Key Laboratory of Bioinorganic and Synthetic Chemistry, State Key Laboratory of Optoelectronic Materials and Technologies, School of Chemistry and Chemical Engineering, Sun Yat-Sen University, Guangzhou 510275, China

[b] Instrumental Analysis & Research Center, Sun Yat-Sen University, Guangzhou 510275, China

* zhangjp7@mail.sysu.edu.cn.

Supplementary Index

Materials and methods

Materials and Methods.

Hip [W. Paw, R. Eisenberg, *Inorg. Chem.*, **1997**, 36, 2287] and $[Ru(Hip)_3]Cl_2$ [J.-Z. Wu, L.-N. Ji, *Transition Met. Chem.* **1999**, *24*, 299] were synthesized according to literature methods. Other reagents and solvents were commercially available and used without further purification.

Inductively coupled plasma atomic emission spectrometry (ICP-AES) data were obtained by a TJA IRIS(HR) instrument. Powder X-ray diffraction (PXRD) patterns were recorded using a Bruker D8 ADVANCE X-ray powder diffractometer (Cu Kα). Thermogravimetry (TG) analyses were performed using a TA Q50 instrument with a heating rate of 5.0 °C/min under dinitrogen flow. Gas sorption isotherms were measured on a Belsorp MAX volumetric adsorption apparatus. The sample was placed in the sample tube and dried under high vacuum at 100 °C for 4 h to remove the remnant solvent molecules prior to measurements.

Photoluminescence measurement. Steady state photoluminescence spectra and lifetime measurements were performed on an Edinburgh FLS920 spectrometer equipped with a continuous Xe900 Xenon lamp and a 405 nm-laser flash lamp. All instrument parameters such as excitation split, emission split, and scanning speed were fixed during the *in situ* measurements. Oxygen responses of photoluminescence were measured in a sealed chamber equipped with quartz windows and a three-way valve which connects the chamber to a vacuum pump and an O_2 cylinder.

Syntheses of $[Ru_xZn_{7-x}(ip)_{12}](OH)_2$·guest (*x*Ru:MAF-34·g). Stirring the mixture of $Zn(OH)_2$ (0.7-0.1x_{feed} mmol), $Ru(Hip)_3Cl_2$ (0.1x_{feed} mmol), Hip (0.264 g, 1.2 mmol), ethanol (EtOH, 40 mL), and $NH_3·H_2O$ (25%, 1.25 mL) in a 50-mL Teflon-lined reactor at room-temperature for 3 days, and 140 °C for 4 days. The resultant orange microcrystalline powder was washed with

EtOH for three times and then immersed in EtOH for 1 day, and finally filtered and dried in air (yield 80~85% based on Zn). The doping ratios were determined by ICP-AES with the digested samples (in 4:1 HNO_3/H_2O_2 at 190 ºC for 30 min), which gave $x_{product}$ = 0.10, 0.13, 0.15, 0.16, 0.29 for five samples synthesized with x_{feed} = 0.16, 0.20, 0.27, 0.30, 0.50, respectively. Potentiometric titration showed that the digested samples contained negligible amount of chloride ion.

It should be noted that single crystals of the archetypal compound MAF-34·g is very difficult to synthesize. As previously reported by us, single crystals of MAF-34·g were synthesized under solvothermal conditions with $Zn(NO_3)_2$, Hip, and trimethylamine/propylamine, Nevertheless, the NO_3^- and amine agent influenced the sorption and luminescent properties seriously. Microcrystalline samples of MAF-34·g can be synthesized effectively by replacing $Zn(NO_3)_2$ and the amines with $Zn(OH)_2$ and aqueous ammonia, respectively. We had tried many times but failed to obtained single crystals of *x*Ru:MAF-34·g under these conditions mentioned above.

We also attempted but failed to prepare *x*Ru:MAF-34·g by using MAF-34·g as a starting material through ion exchange.

Fabrication of luminescent thin films. A CH_2Cl_2 solution of room temperature vulcanized silicone rubber (Momentive TSE-397-C, 50 wt%) was sprayed onto the substrate (glass slice or surface of the blue-light LED) with a spray gun. A suspension of *x*Ru:MAF-34·g (0.010 g) in EtOH (10 mL) was sprayed onto the silicone-rubber layer before it was completely solidified. After that, the film was treated in vacuum for 10 minutes.

Calculation/Description of photoluminescence quenching.

In common luminescent oxygen sensing systems, the bimolecular collision luminescence

quenching can be described by the Stern-Volmer equation

$$\frac{I_0}{I} = \frac{\tau_0}{\tau} = 1 + \frac{4}{1000}\pi\sigma\alpha N_A \tau_0 D_{O_2} S_{O_2} P_{O_2} = 1 + K_{SV} P_{O_2} \quad \text{(eq-S1)}$$

where I_0/τ_0 and I/τ are the luminescent intensity/lifetime in the absence and presence of quencher, respectively, σ is the collision radius of the oxygen-sensing dye, α represents the probability that a collision leads to quenching, N_A is Avogadro's number, D_{O2} is the diffusion coefficients of oxygen, S_{O2} is the oxygen solubility, P_{O2} is the oxygen pressure, and K_{sv} is a combinational constant describing the quenching efficiency of the system. It can be seen that, besides the luminescence lifetime, the diffusion speed and solubility of oxygen in the porous solid are also fundamental parameters determining the quenching efficiency.

A heterogeneous system with two kinds of quenching centers (two luminescence lifetimes) show nonlinear Stern-Volmer plots, which can be described by the modified Stern-Volmer equation

$$\frac{I_0}{I} = \left(\frac{f_1}{1 + K_{SV1} P_{O_2}} + \frac{f_2}{1 + K_{SV2} P_{O_2}} \right)^{-1} \quad \text{(eq-S2)}$$

where f_1 and f_2 ($f_1 + f_2 = 1$) are the fractions of the total emission from the first and second components under unquenched conditions, and K_{SV1} and K_{SV2} are the associated Stern-Volmer quenching constants, respectively.

The relationship between I_0/I and P_{O2} can be written in a linear format

$$\ln\left(\frac{I_0}{I} - 1 \right) = \ln K'_{SV} + \frac{1}{n} \ln P_{O_2} \quad \text{(eq-S3)}$$

where K'_{sv} can be regarded as a quenching constant, n is an empirical parameter, which is obtained by assuming that the quenching behavior is controlled by a Freundlich adsorption

isotherm of oxygen described by the following equation

$$\frac{I_0}{I} = 1 + K'_{SV} P_{O_2}^{1/n} \qquad \text{(eq-S4)}$$

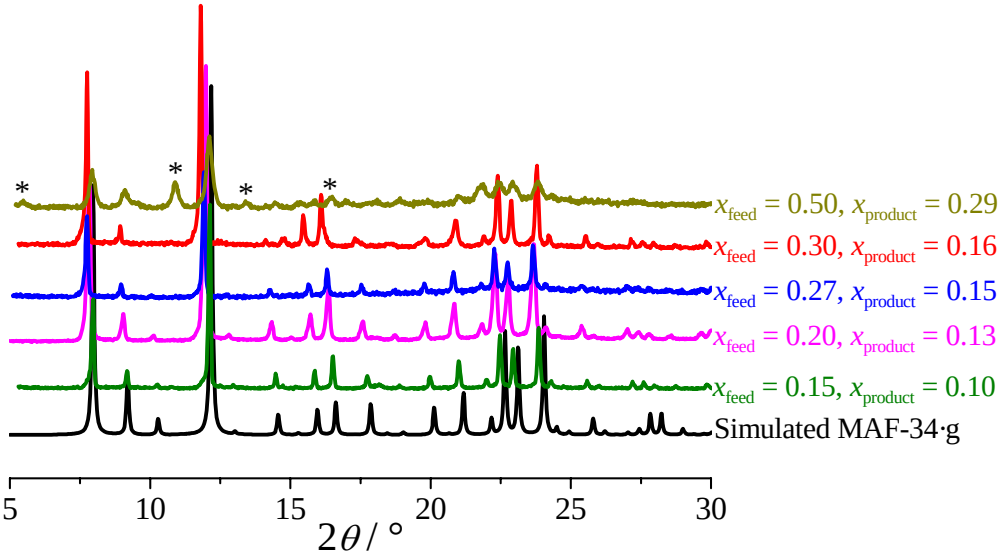

Fig. S1. Comparison of the PXRD patterns of MAF-34·g and microcrystalline samples obtained by Ru doping (peaks of impurities are marked with *). The sample synthesized with x_{feed} = 0.50 displayed significantly widened diffraction peaks, and some unidentified peaks appeared. The Zn/Ru molar ratios of the five obtained products were determined to be 71, 52, 46, 44, 23, corresponding to $x_{product}$ = 0.10, 0.13, 0.15, 0.16, 0.29 or Ru doping efficiency $x_{product}/x_{feed}$ = 67%, 65%, 55%, 53%, 58%, respectively. Except for the highest x_{feed} value, the higher Ru feeding ratio leads to lower doping efficiency, which is consistent with the difficulty of replacing Zn by Ru. Obviously, the sample with $x_{product}$ = 0.29 deviates significantly from MAF-34·g in structure and purity. Therefore, only four samples with $x_{product}$ = 0.10-0.16 were chosen in the subsequent studies.

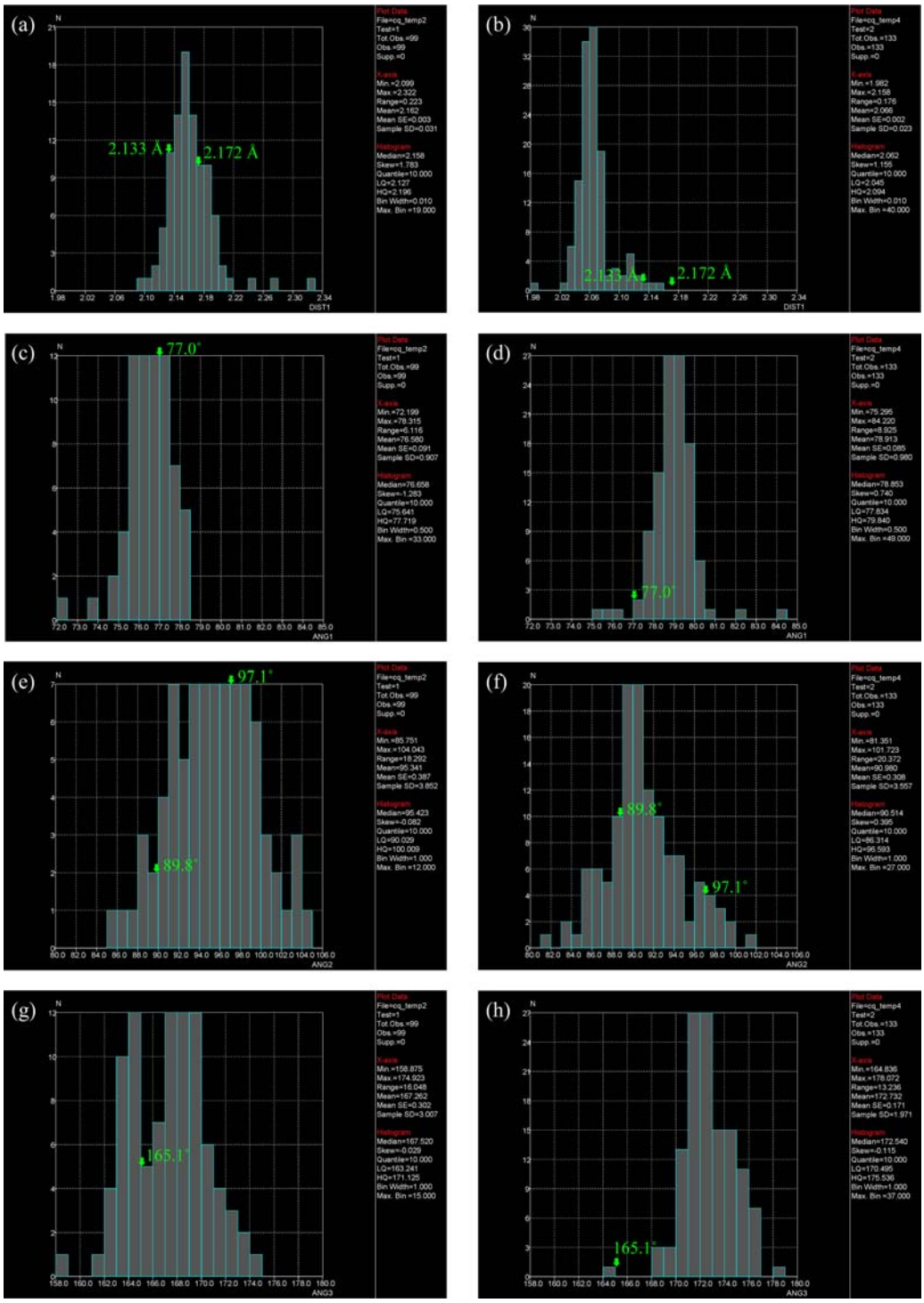

Fig. S2 Statistic comparison of the coordination geometries of $Zn^{II}(bpy)_3$ and $Ru^{II}(bpy)_3$ type complexes. Data were adopted from the Cambridge Structural Database. Bond lengths: (a) Zn-N (b) Ru-N. Cis bond angles of the same ligand: (c) N-Zn-N (d) N-Ru-N. Cis bond angles of different ligands: (e) N-Zn-N (f) N-Ru-N. Trans bond angles: (g) N-Zn-N (h) N-Ru-N. The crystallogarphic values observed for MAF-34·g were marked (green) in the figures.

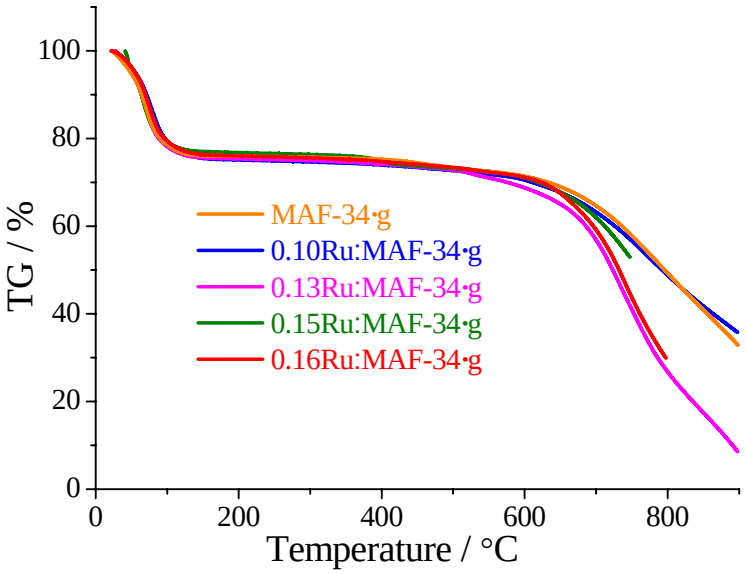

Fig. S3 TG curves of MAF-34·g and *x*Ru:MAF-34·g. TG analyses of *x*Ru:MAF-34·g showed complete removal of the guest molecules with weight losses 20-22% below 140 °C and long plateaus until 600 °C, all of which are similar to MAF-34.

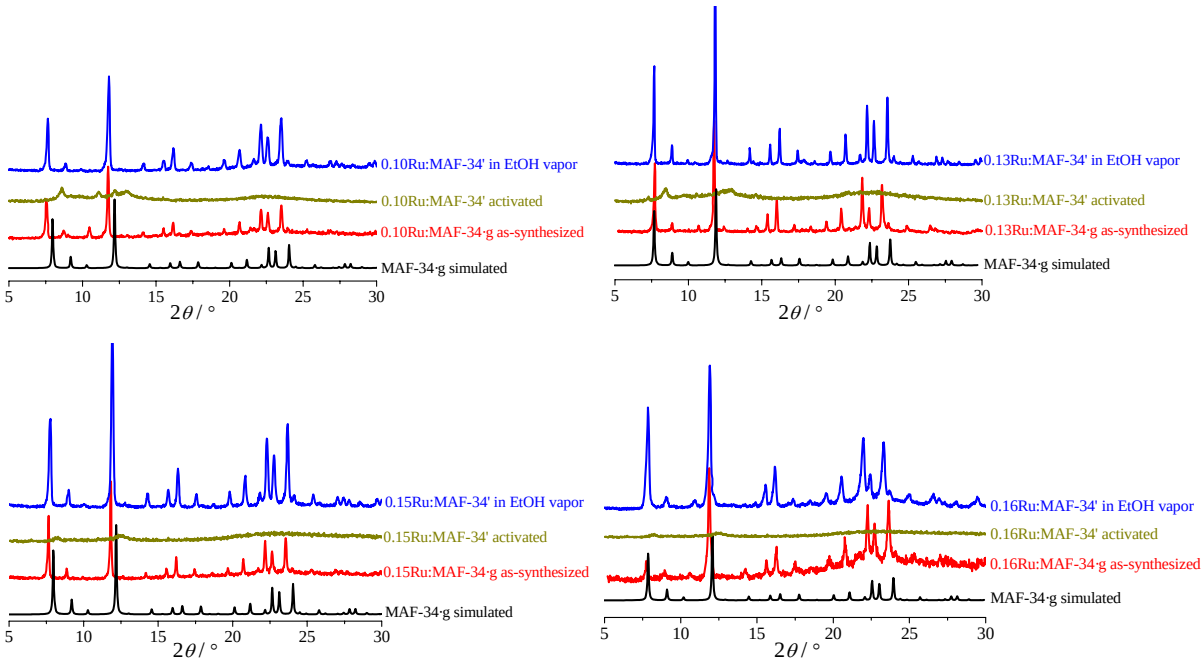

Fig. S4 PXRD patterns showing the interconversion between *x*Ru:MAF-34·g and *x*Ru:MAF-34'. Removal of guest molecules by activation at 200 °C or degassing at room temperature led to significant broadening and weakening of the diffraction peaks. The quasi-amorphous solvent-free *x*Ru:MAF-34' can be reversed to the original structures by reintroducing EtOH. These host-guest behaviors are similar to those of MAF-34

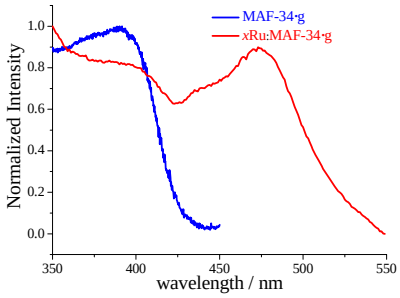

Fig. S5 Excitation spectra of MAF-34·g (λ_{em} = 480 nm) and *x*Ru:MAF-34·g (λ_{em} = 587 nm).

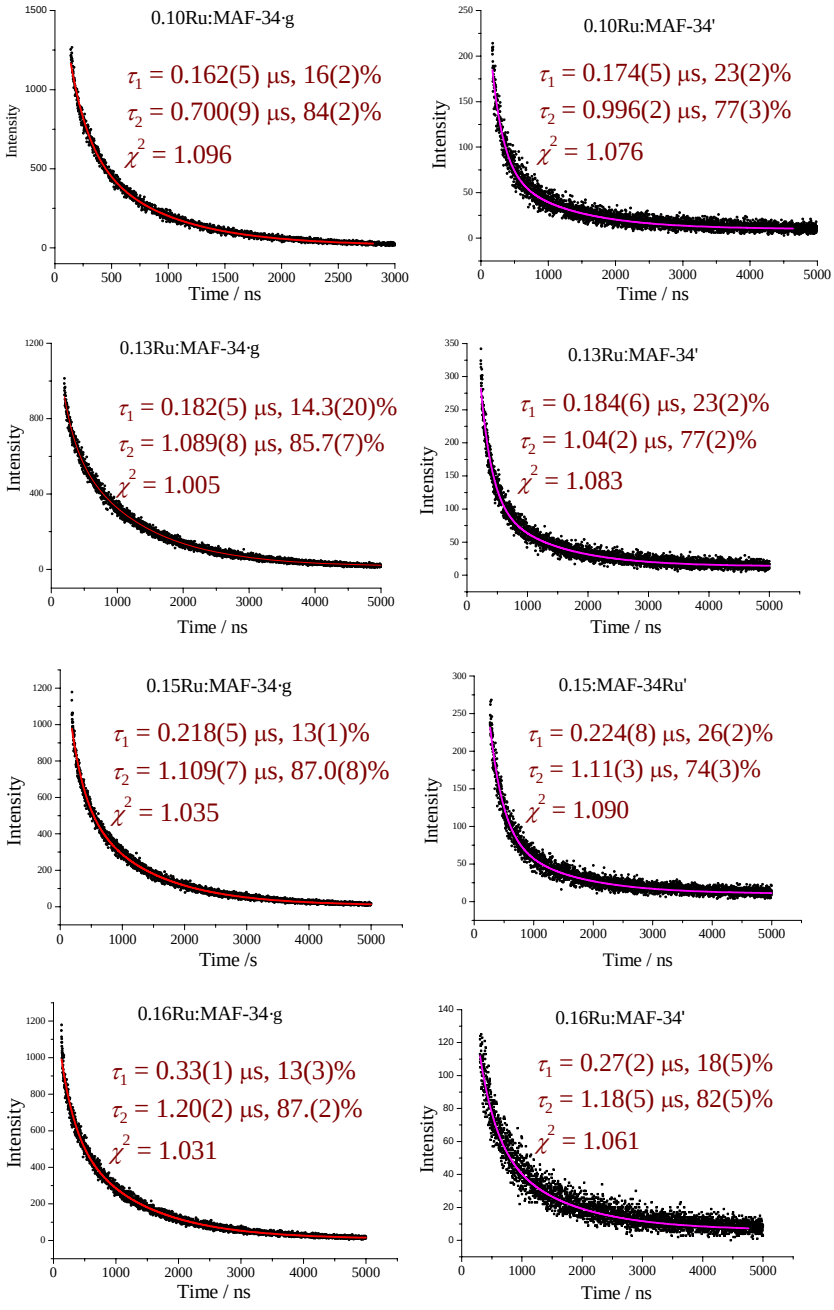

Fig. S6 Luminescence decay profiles and fittings of *x*Ru:MAF-34·g and *x*Ru:MAF-34'.

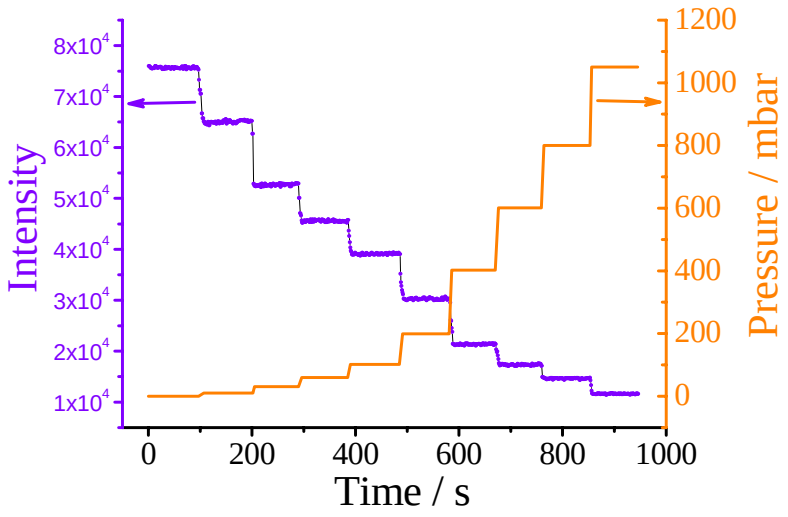

Fig. S7 Dynamic luminescence response and rapid equilibration for 0.16Ru:MAF-34' toward pressure change of O_2. In addition to the quenching efficiency, the quenching speed toward guest pressure change is also important. The luminescence intensity changes in exactly the same trend as the pressure does, indicating very fast luminescence response.

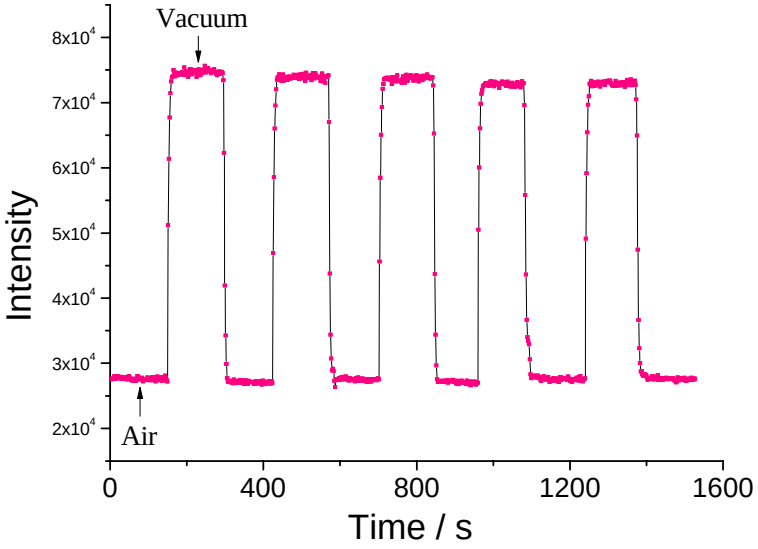

Fig. S8 Repeated luminescence responses of 0.16Ru:MAF-34' in vacuum and Air.

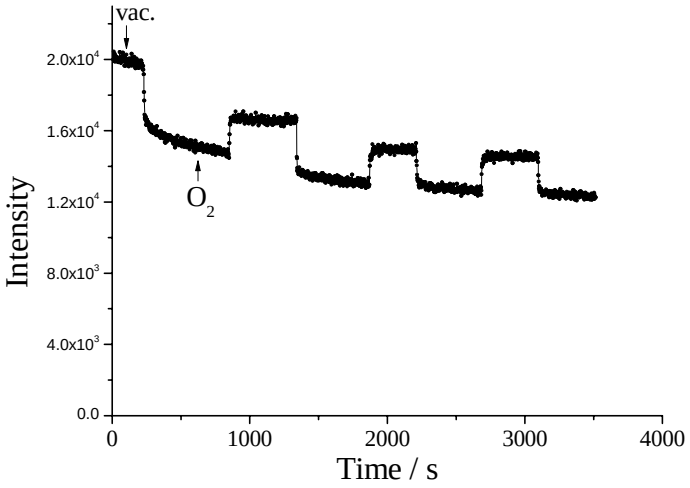

Fig. S9 Variation of the luminescence intensity of $Ru(Hip)_3Cl_2$ upon alternating exposure to O_2 (1 atm) and vacuum.

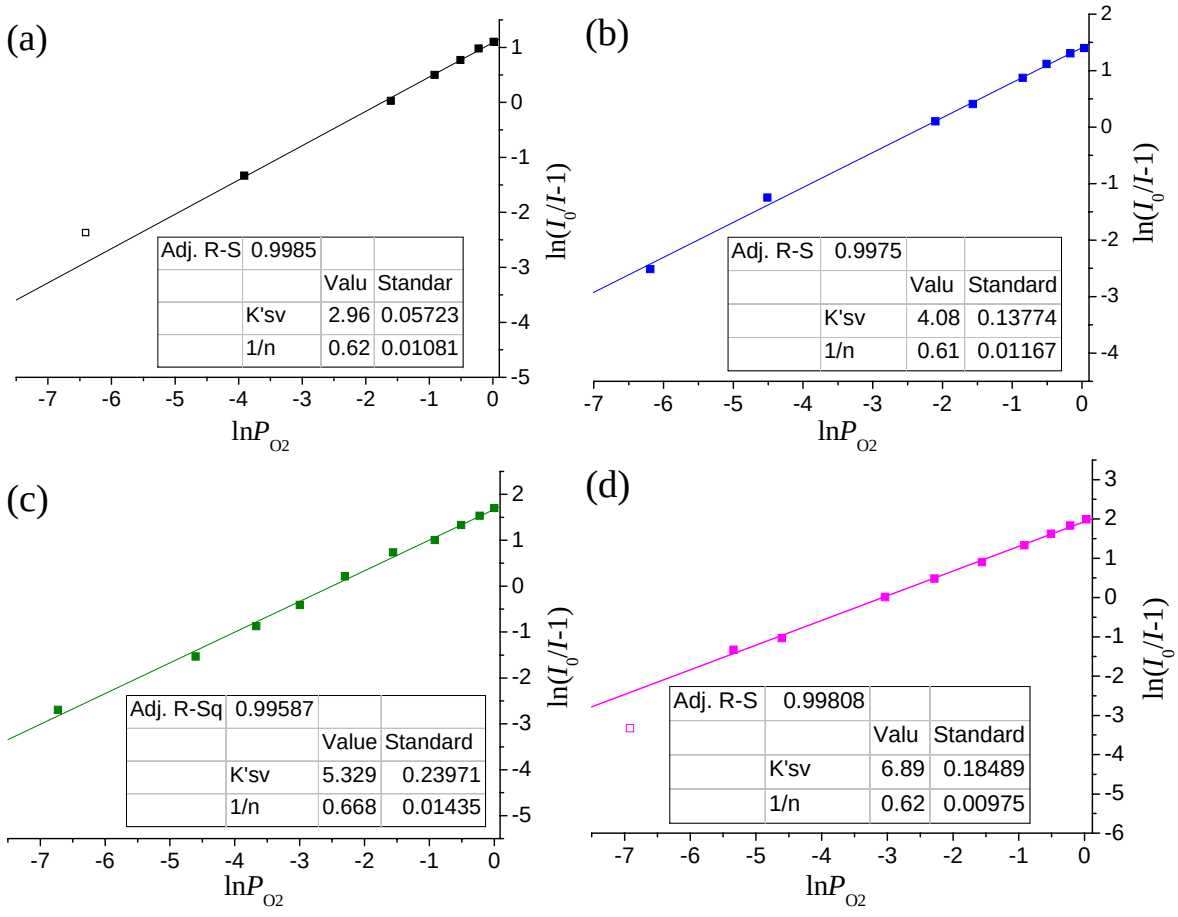

Fig. S10 Linear fitting (the solid symbols are used) of the quenching data of *x*Ru:MAF-34' according to the Freundlich isotherm model. (a) $x = 0.10$, (b) $x = 0.13$, (c) $x = 0.15$, (d) $x = 0.16$.

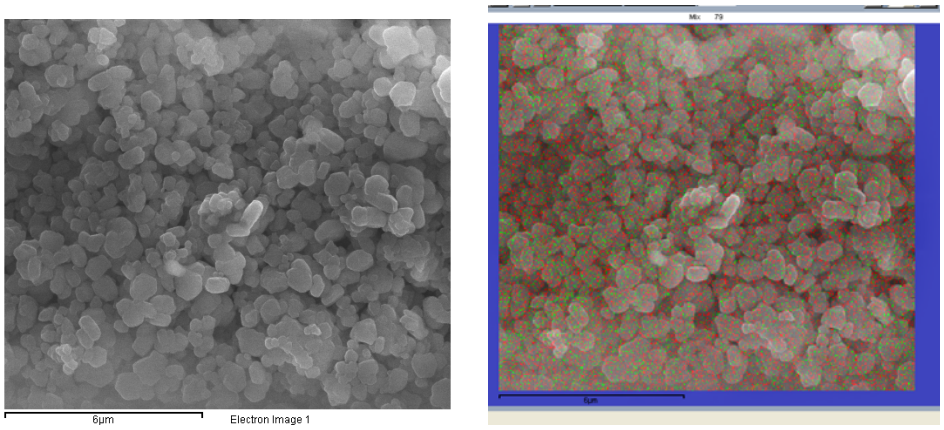

Fig. S11 SEM image (left) and the EDX mapping (right, red: Zn; green: Ru) of the luminescent thin film composed of microcrystalline 0.16Ru:MAF-34'.

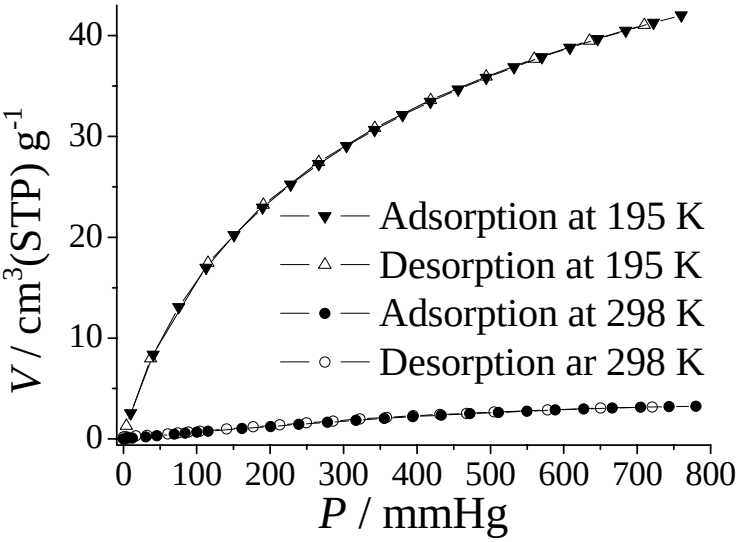

Fig. S12 O_2 sorption isotherms of 0.16Ru:MAF-34'. The O_2 sorption isotherm of 0.16Ru:MAF-34' measured at 195 K gave a pore volume of 0.065 cm^3 g^{-1} and a Langmuir surface area of 173 m^2 g^{-1}, which are similar to those of MAF-34'.

Table S1. Luminescence quenching parameters of *x*Ru:MAF-34'.

x	0.10	0.13	0.15	0.16
λ_{em}/nm	595	600	603	609
I_0/I_{100}	4.01	5.04	6.48	8.3
E_q	75%	80%	85%	88%
K_{sv1}/bar^{-1}	0.31(6)	0.51(4)	1.09(5)	0.96(6)
K_{sv2}/bar^{-1}	8.5(6)	15.4(10)	23(2)	25(1)
f_1	0.22(2)	0.23(2)	0.26(2)	0.18(5)
τ_1/μs	0.174(5)	0.184(6)	0.224(8)	0.27(2)
f_2	0.78(3)	0.77(2)	0.74(3)	0.82(5)
τ_2/μs	0.996(2)	1.04(2)	1.11(3)	1.18(5)
K'_{sv}	2.97(6)	4.1(1)	5.3(2)	6.9(2)